OLED4-3L
Late-News Paper
Invited

Analysis of Emission Zone Profile in an Organic–Quantum Dots Hybrid Device

Hin-Wai Mo[1], Kentaro Harada[2,3], Chihaya Adachi[1,3]

h-mo@ist.or.jp
[1] Fukuoka i^3-Center for Organic Photonics and Electronics Research (i^3-opera), Fukuoka, Japan
[2] OPERA Solution Inc., Fukuoka, Japan
[3] Center for Organic Photonics and Electronics Research (OPERA), Kyushu University, Fukuoka, Japan

Keywords: Quantum Dot; Quantum Dot Light-Emitting Diodes (QLEDs); Emission Zone Profile (EZP)

ABSTRACT

We report first time the emission zone profile, the spatial distribution of the emission intensity along the direction of the applied bias, of a quantum dot light-emitting diode. The emission zone profile is correlated with the balance of n- and p-type currents in a diode, and the device efficiency and its roll-off behavior strongly depend on whether the emission peak is preferably distributed or concentrated at a specific interface. The emission zone profiling can thus provide us with clues for improving the performance of organic–quantum dots hybrid devices.

1 Introduction

Colloidal quantum dots (QDs) have recently been attracting much attention as one of the most promising next generations emitting materials [1-4]. While QD device performances have been improved in recent years, e.g., with their external quantum efficiency (EQE) from less than 0.01 % to over 20 %, there are still rooms for further progress in terms of both material development and device physics [5-6]. Besides the stability and the quantum yield of QD emitters, the charge carrier balance in a device as well as the alignment of transport energy levels in a multi-layered stack is also critical issues to be considered [7].

We have recently developed a method of emission zone analysis based on a single emission spectrum measurement [8-9]. In this method, by accurately controlling the thickness of an organic light-emitting diode (OLED), we deliberately prepare an experimental sample having a destructive interference. The light spectrum outcoupled from such a destructive interference sample depends strongly on the spatial distribution of the emission in the emission layer (EML). Therefore, by fitting of an adequate equation and the corresponding parameters to the experimental spectrum, the emission zone profile of an OLED can be obtained.

We utilize an inverted quantum dot light-emitting diode (QLED) as the experimental model in this work. By visualizing the emission zone profiles of QLEDs, we discuss the balance of *n*- and *p*-type currents and the resultant recombination site in the EML of the QLEDs. The findings demonstrate that the emission zone profiling is a competent method which helps us understand the efficiency loss mechanism in a QLED and hence expand possibilities for further improvement of the future device performance.

2 Experiment

Materials: The QLED architecture used in this study was composed of zinc oxide (ZnO) or magnesium-substituted ZnO (ZnMgO) nanoparticles (purchased from NS materials and Mesolight Inc., respectively) as the electron transport layer (ETL), indium phosphide (InP)-based QDs (purchased from Mesolight Inc.) as the EML, 4,4',4''-Tri(9-carbazoyl)triphenylamine (TCTA) as the electron blocking layer (EBL), 9-Phenyl-3,6-bis(9-phenyl-9Hcarbazol-3-yl)-9H-carbazole (Tris-PCz) and 2,3,6,7,10,11-Hexacyano-1,4,5,8,9,12-hexaazatriphenylene (HAT-CN) as the hole transporting layer (HTL) and hole injection layer (HIL), respectively. All materials were used as provided.,

Device fabrication: The devices were prepared on cleaned glass substrates patterned with indium-doped tin oxide (ITO). All the spin-coating processes were carried out in a nitrogen-filled glovebox. The electron transport nanoparticles (ZnO or ZnMgO) solutions were spin-coated onto ozone-treated ITO substrates at 3,000 rpm for 30 sec and then baked at 135 °C for 15 min. The QD solutions were subsequently spin-coated at 3,000 rpm for 30 sec and baked at 135 °C for 15 min. The spin-coated substrates were loaded into a deposition chamber with the base pressure of ~10^{-6} Pa. The active device areas (4 mm^2) of the QLEDs were defined by the overlapping region of the ITO anode and the aluminum (Al) cathode. After the QLED fabrication, all the devices were encapsulated under nitrogen ambient with cover glasses using a UV-curable adhesive.

For the device characterization and the emission zone analysis described in the below subsection, two sets of devices with constructive interference (named the optimized devices) and destructive interference (named the dark devices) were fabricated. The destructive interference devices were fabricated by intentionally changing the thickness of the charge transport layers (explained more in Results ad Discussion section).

Device characterization and emission zone analysis: Current density–voltage–luminance (J–V–L) data were measured with a Keithley 2400 source meter and absolute EQE measurement system (C9920-12, Hamamatsu Photonics, Japan) with an optical fiber connected to a photonic multichannel analyzer (PMA-12, Hamamatsu Photonics). Setfos commercial software version 4.6 from Fluxim AG was used for optical simulations. Low-energy inverse photoemission spectroscopy (LEIPS) was carried out by using PHI5000 VersaProbe III scanning ESCA microprobe at ULVAC PHI, Inc [10].

For the emission zone fitting, the substrate normal (0-degree) outcoupling spectrum measured from the dark device was considered as the far field intensity, *I*, i.e., the solution of the linear equation

$$I_{\lambda_j,\theta_i} = \sum_{m=1}^{N} A_{\lambda_j,\theta_i}(z_m) \times M_{\lambda_j} \times \rho(z_m) \times \Delta z \ , \quad (1)$$

where *A* is the emission energy distribution simulated by Setfos, *M* is the intrinsic QD spectrum, ρ is the weights of emission at a discrete position, Δz is the position step size, λ_j is the wavelength, θ_i is the observation angle and z_m is the emitter position. All the parameters except ρ were known before the fitting. Further details of the emission zone analysis method can be found in our previous paper [9].

3 Results and Discussion

Normally, a light-emitting diode is designed to have a microcavity with constructive interference so that it achieves the maximum outcoupling efficiency at 0˚ (normal to the substrate). In this case, the spectral shape of the 0˚ light is not sensitive to the position of the emission zone, i.e., the position in the EML, from where the most of radiating dipoles are originating. Note that an outcoupling light spectrum generally has an angular dependency for a strong cavity, but it is another issue since we here focus on 0˚ light only. On the other hand, the 0˚ spectral shape of a dark device with destructive interference is very sensitive to the emission zone distribution, meaning that a small shift in the peak position of radiating dipoles would lead to a large deformation of the 0˚ spectrum.

For experimental demonstration, two types (optimized and dark) of inverted red QLEDs are fabricated. The structure of the optimized device is as follows: ITO (anode)/ZnO (ETL, 45 nm)/QD (EML, 20 nm) /TCTA (EBL, 10 nm) / Tris-PCz (HTL, 40 nm) /HAT-CN (HIL, 10 nm)/Al (cathode). The structure of the dark device is essentially the same with that of the optimized device except that an additional layer of 97 nm-thick Tris-PCz doped with HAT-CN is inserted between HTL and HIL just as an optical spacer. The conductivity of the *p*-doped additional layer is so high that it has no significant impact on the electrical property of the QLED. Figure 1a and 1b indeed shows that the J–V characteristics of the dark (with a *p*-doped spacer) and the optimized devices are identical. The emission zone profile obtained from the dark device is therefore a reasonable measure to discuss the real emission zone in the optimized QLED with constructive interference.

Figure 1c shows the 0˚ spectra measured from the dark devices in black dashed lines. The fitting results using Eq. (1) are shown in red solid-lines. The green bar charts under the spectral graphs are the fitting results, indicating the weights of emission at each discrete position within the EML. The emission zone profiling at different current densities, 0.024 mA·cm^{-2} (under turn-on bias), 1 mA·cm^{-2}, 10 mA·cm^{-2} and 50 mA·cm^{-2} are compared in Fig. 1c. The results show that the emission peaks of the QLEDs are concentrated at the HTL/EML interface in all driving currents.

The concentrated and narrow emission zone profiles can be first explained by a high electron transport ability of the QD nanoparticles. The high electron mobility of an InP-based QD has been reported as 0.45 cm^2·V^{-1}·s^{-1} [11], while almost no report on InP-QD hole mobility is found from literature. The very flat valence band in a bulk InP Brillouin zone [12] suggest that the effective mass of a hole is quite large. Although the conduction mechanism through QD particles (thermal activation due to the shell and the ligand spaces) is complex, it is reasonable to assume that the electron mobility in an InP-based QD layer is far higher than the hole mobility. Therefore, our inverted QLED has a tendency that the recombination zone is forced to reside at the HTL/EML interface.

Besides, the balance of *n*- and *p*-type currents in a diode is also regulated by the ability to provide electrons and holes from ETL and HTL, respectively, to the EML. The electron mobility of ZnO nanoparticles (ETL) is on

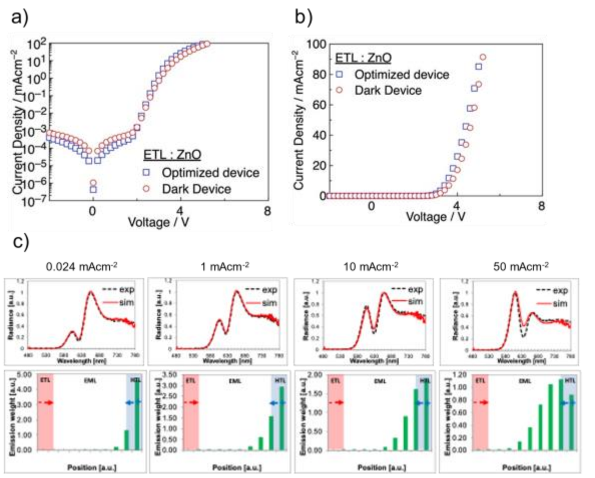

Fig. 1 Comparison of J–V characteristics between the optimized device (blue square) and the dark device (red circle) in a) semi-log scale and b) linear scale. c) Results of emission zone profiling of a QLED for various current density conditions. The upper graphs show 0˚ outcoupling spectra from the dark device (black dotted lines) and the fitting curves (red solid lines). Lower graphs show the weights of emission at each discrete position in the EML.

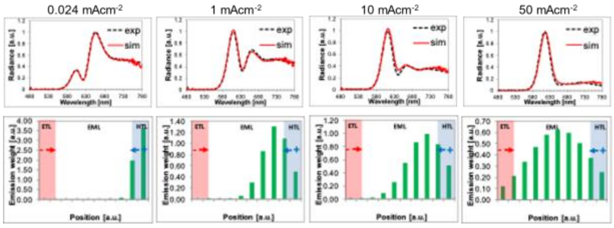

Fig. 2 Results of emission zone profiles of a QLED with ZnMgO ETL for various current density conditions.

the order of 10^{-4} $cm^2 \cdot V^{-1} \cdot s^{-1}$ [13-14], and the hole mobility in a Tris-PCz film (HTL) is around10^{-5} $cm^2 \cdot V^{-1} \cdot s^{-1}$ [15]. Note that the provision of charge carriers is not described by mobility but conductivity. Electrical conductivity, σ, is given by the expression

$$\sigma = ne\mu_e + pe\mu_h \ , \qquad (2)$$

where *n* and *p* are the electron and hole, respectively, densities, μ_e and μ_h are the electron and hole, respectively, mobilities and *e* is the elementary charge. The Tris-PCz (HTL, not the *p*-doped optical spacer) layer in our devices is undoped and is electrically an insulator. On the other hand, we found a relatively high conductivity of 4.1 x 10^{-5} $S \cdot cm^{-1}$ in our ZnO nanoparticle film, suggesting that an excessively high electron density is injected into our EML and therefore, the *n*-type current always prevails the *p*-type one in the EML.

To adjust the balance of *n*- and *p*-type currents, we considered to replace the ETL by another one having a low conductivity that is comparable with or even lower than that of the HTL. Wang et al. reported that the mobility of $Zn_{0.85}Mg_{0.15}O$ nanoparticles is around 10^{-6} $cm^2 \cdot V^{-1} \cdot s^{-1}$, and insertion of a ZnMgO interlayer can improve the QLED performance by regulating the electron transport from the ETL to the EML. A systematic study on the properties on ZnMgO nanoparticles by Kılınç et al. revealed that substitution of Zn ions by Mg ions decreases the conductivity from 10^{-5} down to 10^{-9} $S \cdot cm^{-1}$ [16]. Zhang et al. and Li et al. have also recently improved the QLED performance by utilizing ZnMgO ETL [17-18]. We indeed confirmed that the conductivity of a ZnMgO film was lower than the detection limit of the source meter. In addition, LEIPS measurements were performed to compare the energetics of ZnO nanoparticles and ZnMgO nanoparticles. While the energetic distance between the electron affinity, *X*, and the Fermi level, E_f, of the ZnO film is only 0.05 eV, E_f of the ZnMgO film is 0.37 eV away from the conduction level, implying a very low free electron density in ZnMgO due to deep donor states created by the Mg substitution, suggesting that ZnMgO is a suitable candidate to replace the current ZnO ETL.

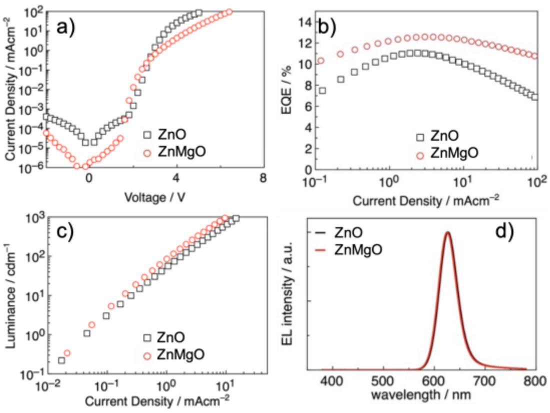

Fig. 3 Device characteristics of QLEDs with ZnO ETL and ZnMgO ETL; a) J–V plots, b) EQE–J plots, c) L–J plots and d) electroluminescence spectra.

Based on the consideration above, we fabricated optimized and dark devices with the ETL replaced by ZnMgO, the other QLED structure being the same with the previous ones. The results of emission zone analysis for various current density conditions are shown in Fig. 2. Under lower current densities (see, e.g., 0.024 $mA \cdot cm^{-2}$), the emission zone is concentrated at the HTL/EML interface, which is inevitable due to the nature of InP-based QDs having a high electron mobility. However, as the current density increases, the emission peak is shifted toward the center of the EML and the distribution of the emission weights is spread wider across the EML (see 50 $mA \cdot cm^{-2}$). This clearly indicates that the injection of electrons is regulated by the low conductivity ZnMgO ETL, which is the electrical constraint of this system. According to Eq. (2), the higher the total carrier density is injected, the higher the ratio of *p*-type to *n*-type current is achieved. The trend shown in Fig. 2 is advantageous in the sense that a risk of too high exciton concentration at the HTL/EML interface would be avoided especially for higher current densities.

The comparison of the optimized device characteristics between the original QLED with ZnO ETL and the modified QLED with ZnMgO ETL are shown in Fig. 3. The J–V characteristics in Fig. 3a prove that the ZnMgO ETL has indeed a lower conductivity, resulting in roughly one order of magnitude lower current density than for the original device. Figure 3b compares the EQE versus J plots of the two devices. The modified QLED with ZnMgO ETL shows a superior EQE in overall current range and especially, the roll-off at the higher current range is suppressed compared to the original QLED. The strong role-off observed for the original QLED should be attributed to an interfacial quenching due to a concentration of the emission zone, which is a result of an *n*-type current domination in the EML. The results of the device characteristics shown here are well consistent with the consideration of the ZnO/ZnMgO energetics and the prediction by the emission zone analysis (Fig. 2). Thus, emission zone analysis is proven to exactly reflect the electrical properties of an organic–QD hybrid device.

4 Conclusions

By utilizing a unique analytical method, the emission zone profiles of an organic–QD hybrid system were first time visualized. The emission zone of our inverted QLED was forced to be concentrated due to a domination of the *n*-type current in the EML. The imbalance of *n*/*p* current ratio was improved by controlling the conductivity of the ETL, drastically improving the device EQE and suppressing the roll-off. The insights obtained from the emission zone analysis are valuable for understanding the device physics in QLEDs. We expect that the method to combine the emission zone analysis and the electrical device tuning will accelerate development of high-performance and long-lived organic–QD hybrid devices.

5 Acknowledgement

We thank Masahiro Terashima, Shinichi Iida and Takuya Miyayama of ULVAC-PHI, Inc. for the LEIPS measurements.

References

[1] X. Dai, Z. Zhang, Y. Jin, Y. Niu, H. Cao, X. Liang, L. Chen, J. Wang & X. Peng, "Solution-processed, high-performance light-emitting diodes based on quantum dots," Nature 96, 515 (2014).

[2] Y. Yang, Y. Zheng, W. Cao, A. Titov, J. Hyvonen, J. R. Manders, J. Xue, P. Holloway & L. Qian, "High-efficiency light-emitting devices based on quantum dots with tailored nanostructures," Nat. Photon. 9, 259 (2015).

[3] Z. Zhang, Y. Ye, C. Pu, Y. Deng, X. Dai, X. Chen, D. Chen, X. Zheng, Y. Gao, W. Fang, X. Peng, Y. Jin, "High-performance, solution-processed, and insulating-layer-free light-emitting diodes based on colloidal quantum dots," Adv. Mater. 30, 1801387 (2018).

[4] Ki. Lee, Chang. Han, H. Kang, H. Ko, C. Lee, J. Lee, N. Myoung, S. Yim, and H. Yang, "Highly efficient, color-reproducible full-color electroluminescent devices based on red/green/blue quantum dot-mixed multilayer," ACS Nano 9(11), 10941 (2015).

[5] H. Zhang, N. Hu, Z. Zeng, Q. Lin, F. Zhang, A. Tang, Y. Jia, L. Li, H. Shen, F. Teng, Z. Du, "High-efficiency green InP quantum dot-based electroluminescent device comprising thick-shell quantum dots," Adv. Optical Mater. 7, 1801602 (2019).

[6] W. Zhang, W. Zhuang, X. Qu, H. Liu, K. Wang, X. Wei Sun, "High quantum yield InP/ZnMnS/ZnS quantum dots," SID Symposium Digest 50, 1716 (2019).

[7] C. Ippen, W. Guo, D. Zehnder, D. Kim, J. Manders, D. Barrera, B. Newmeyer, D. Hamilton, C. Wang, C. Hotz, R. Ma, J. Bin, B. Kim, K. Kim, K. Jang, J. Park, T. Lee, W. Kim, J. Lee, "High efficiency heavy metal free QD-LEDs for next generation displays," J. Soc. Inf. Display. 27, 338 (2019).

[8] R. M. Ciarnáin, H. W. Mo, K. Nagayoshi, H. Fujimoto, K. Harada, T. H. Ke, P. Heremans, C. Adachi, "Emission zone measurement gives insight into the suitability of accelerated ageing extrapolation," IDW 2020, 415 (2020).

[9] R. M. Ciarnáin, H. W. Mo, K. Nagayoshi, H. Fujimoto, K. Harada, R. Gehlhaar, T. H. Ke, P. Heremans, C. Adachi, "A thermally activated delayed fluorescence green OLED with 4500 h lifetime and 20% external quantum efficiency by optimizing the emission zone using a single-emission spectrum technique," Adv. Mater. 34, 2201409 (2022).

[10] H. Yoshida, "Near-ultraviolet inverse photoemission spectroscopy using ultra-low energy electrons," Chem. Phys. Lett., 539, 180 (2012).

[11] T. Zhao, Q. Zhao, J. Lee, S. Yang, H. Wang, M. Chuang, Y. He, S. M. Thompson, G. Liu, N. Oh, C. Murray, C. Kagan, "Engineering the surface chemistry of colloidal InP quantum dots for charge transport," Chem. Mater. (2020).

[12] M. Niu, D. Cao, K. Sui, C. Liu, "InP/TiO2 heterojunction for photoelectrochemical water splitting under visible-light," International Journal of Hydrogen Energy 45, 11515 (2020).

[13] N. Kirkwood, B. Singh, P. Mulvaney, "Enhancing quantum dot LED efficiency by tuning electron mobility in the ZnO electron transport layer," Adv. Mater. Interface 3, 1600868 (2016).

[14] L. Wang, J. Lin, X. Liu, S. Cao, Y. Wang, J. Zhao, B. Zou, "Mg-doped ZnO nanoparticle films as the interlayer between the ZnO electron transport layer and InP quantum dot layer for light-emitting diodes," J. Phys. Chem. C 124, 8758 (2020).

[15] W. Hung, P. Chiang, S. Lin, W. Tang, Y. Chen, S. Liu, P. Chou, Y. Hung, K. Wong, "Balance the carrier mobility to achieve high performance exciplex OLED using a Triazine-based acceptor," ACS Appl. Mater. Interfaces 8, 4811 (2016).

[16] N. Kılınç, L. Arda, S. Öztürk, Z. Z. Öztürk, "Structure and electrical properties of Mg-doped ZnO nanoparticles," Crystal Research & Tech. 45, 529 (2010).

[17] Z. Zhang, Y. Ye, C. Pu, Y. Deng, X. Dai, X. Chen, D. Chen, X. Zheng, Y. Gao, W. Fang, X. Peng, Y. Jin, "High-performance, solution-processed, and insulating-layer-free light-emitting diodes based on colloidal quantum dots," Adv. Mater. 30 1801387 (2018).

[18] D. Li, B. Kristal, Y. Wang, J. Feng, Z. Lu, G. Yu, Z. Chen, Y. Li, X. Li, X. Xu, "Enhanced efficiency of InP-based red quantum dot light-emitting diodes," ACS Appl. Mater. Interfaces 11, 37, 34067 (2019).